

Population distributions from native mass
spectrometry titrations reveal nearest-neighbor
cooperativity in the ring-shaped oligomeric protein

TRAP

Melody L. Holmquist,¹ Elihu C. Ihms,² Paul Gollnick,³ Vicki H. Wysocki,^{1,4} and Mark P. Foster^{1*}*

¹ Department of Chemistry and Biochemistry, The Ohio State University, Columbus, Ohio

² VPPL, Vaccine Research Center, NIAID, NIH, Vaccine Pilot Plant (VPP), Frederick, Maryland

³ Department of Biological Sciences, State University of New York at Buffalo, Buffalo, New
York

⁴ Resource for Native Mass Spectrometry Guided Structural Biology, The Ohio State University,
Columbus, Ohio

Keywords: Native mass spectrometry, ligand-protein allostery, statistical thermodynamic models,
homo-oligomers

ABSTRACT

Allostery pervades macromolecular function and drives cooperative binding of ligands to macromolecules. To decipher the mechanisms of cooperative ligand binding it is necessary to define, at a microscopic level, the thermodynamic consequences of binding of each ligand to its energetically coupled site(s). However, extracting these microscopic constants is difficult for macromolecules with more than two binding constants. This goal is complicated because the observable (e.g., NMR chemical shift changes, fluorescence, enthalpy) can be altered by allostery, thereby distorting its proportionality to populations of states. Because it measures mass, native mass spectrometry (MS) can directly quantify the populations of homo-oligomeric protein species with different numbers of bound ligands, provided the populations are proportional to ion counts and that MS-compatible electrolytes do not alter the overall thermodynamics. These measurements can help decipher allosteric mechanisms by providing unparalleled access to the statistical thermodynamic partition function. We used native MS (nMS) to study the cooperative binding of tryptophan (Trp) to *Bacillus stearothermophilus* *trp* RNA-binding attenuation protein (TRAP), a ring-shaped homo-oligomeric protein complex with 11 identical binding sites. Mass spectrometry-compatible solutions did not significantly perturb protein structure and thermodynamics as assessed by ITC and NMR spectroscopy. Populations of $\text{Trp}_n\text{-TRAP}_{11}$ states were quantified as a function of Trp concentration by native mass spectrometry. Population distributions cannot be explained by a non-cooperative binding model but are well described by a nearest neighbor cooperative model. Non-linear least-squares fitting of the populations to a mechanistic model yielded microscopic thermodynamic constants that define the interactions between neighboring binding sites that result in homotropic cooperativity in Trp binding to TRAP.

Introduction

Allosteric communication between ligand binding sites in homo-oligomeric proteins provides a powerful means of regulating their function.^{1,3} Even for the best characterized homo-oligomeric allosteric proteins, like hemoglobin, the AAA+ proteases⁴ and GroES/GroEL chaperonins,^{5,6} the mechanisms of allosteric communication remain controversial and poorly understood, or described only phenomenologically. Cooperativity is most commonly diagnosed from ligand binding curves that fit poorly to a simple Langmuir isotherm. Sigmoidal curves arising from positive cooperativity can be diagnostic; fitting such data with the Hill equation can provide a numerical descriptor of the steepness of the binding curve. However, the Hill coefficient is phenomenological, cannot be interpreted thermodynamically without further assumptions, and has limited mechanistic value.⁷ To decipher the mechanisms that lead to positive or negative cooperativity in ligand binding, it is necessary to quantify the microscopic thermodynamic linkages between allosteric sites, and the resulting shifts in populations of protein-ligand states.⁸⁻¹²

Mechanistic modeling can provide access to microscopic thermodynamic parameters, but lack of proportionality between experimental observables and liganded state of a cooperative binding lattice complicates thermodynamic analysis. Isothermal titration calorimetry (ITC) is generally the method of choice for characterizing binding thermodynamics, with some important examples of its utility in studying cooperative interactions.¹³⁻¹⁵ ITC directly measures the enthalpy change (ΔH) resulting from binding of a ligand to a macromolecule; fitting the data to an appropriate binding model yields the overall free energy change ΔG via the equilibrium association constant K_d . However, cooperativity can alter each of these thermodynamic parameters, since binding of successive ligands may occur with higher or lower affinity and be more or less enthalpic, and it becomes difficult to disentangle the thermodynamics of overlapping and simultaneous binding events.^{12,16} Moreover, under conditions of high c -value, defined as the ratio between the

concentration of the binding sites to the equilibrium dissociation constant¹⁷, cooperative effects can be easily masked.^{12,16} These complications make it difficult to determine the populations of various liganded states through the course of a titration, and thus to quantify their relative free energies.

Native mass spectrometry (nMS)^{18,19} has the potential to resolve the problem of quantifying liganded populations in oligomeric proteins.^{20,21} Unlike unidimensional metrics like heat, fluorescence intensity, or chemical shift, wherein it might be difficult to discern whether half of the sites on each oligomer are bound, or half of the oligomers are fully bound, the number of bound ligands can be directly read out from the masses of the species. Provided the binding of individual ligands can be resolved under the given experimental conditions, and that the detected signals are proportional to the states present in solution, native MS can provide un-paralleled detail into the populations of accessible ligand-macromolecule states, and therefore the statistical thermodynamic partition function, including microscopic thermodynamic cooperativity parameters.^{21,22}

Under “soft” ionization conditions, nMS preserves the tertiary and quaternary structures of protein complexes, allowing investigation of the stability, conformation, topology, interactions, and stoichiometry of their subunits.^{18,19} In nMS, nano-electrospray ionization is used to produce multiply-protonated protein complexes, comprising a narrow range of charge states, while retaining much of their native tertiary structures in gas phase. Due to the deleterious effects of classic biochemical solutions such as potassium phosphate, Tris and HEPES, macromolecule samples are sprayed from solutions comprising volatile electrolytes, such as ammonium bicarbonate, ammonium acetate (AmAc), or ethylenediamine diacetate (EDDA).²³⁻²⁵ While various gas-phase evidence suggests that protein tertiary and quaternary structures are retained when sprayed from these solutions²⁶⁻²⁸, effects of MS electrolytes on solution structures and ligand binding

affinities remain poorly understood. In literature, there is disparity of solution experiments with MS electrolytes.

We examined the utility of nMS for quantifying populations of liganded states of the oligomeric tryptophan-binding protein TRAP from *Bacillus stearothermophilus*, and for determining microscopic thermodynamic parameters describing its homotropic cooperativity. The *trp* RNA binding attenuation protein (TRAP), forms homo-oligomeric rings (mostly 11-mers), and is capable of binding one tryptophan ligand (Trp) between each pair of protomers in the ring (**Figure 1**). Allostery in TRAP has been the subject of numerous past studies that often yielded conflicting results and fell short of detailed mechanistic insight.²⁹⁻³⁶ Equilibrium dialysis experiments of Trp binding with TRAP from *B. subtilis* yielded apparent binding constants of 5-10 μM , and weak cooperativity via Hill coefficients of 1.5-2.^{36,37} Weak or no cooperativity was found via Hill analysis³⁴ or single-temperature ITC studies of *B. stearothermophilus* TRAP at high c-value.³⁰ In contrast, at lower concentrations, and at different temperatures, multiple mode thermodynamic binding could be discerned.¹² The application of mechanism-based statistical thermodynamic modeling yielded good fits to a nearest-neighbor circular lattice model, and revealed weak thermodynamic coupling between sites. *Bst* and *Bsu* TRAP have also already been shown to retain their quaternary structure in the gas phase,³⁸⁻⁴⁰ validating their use in detailed thermodynamic investigation by nMS.

Here we explored the use of nMS for quantifying cooperativity in Trp binding to *Bst* TRAP. We used heteronuclear NMR and ITC to examine the effect of the MS-compatible solutions AmAc and EDDA on the structure and thermodynamics of Trp binding by *Bst* TRAP, compared charge states and ligand populations of ions in ESI-MS generated from EDDA and AmAc solutions, examined charge-state dependence of liganded populations, measured ligand-dependent population shifts during replicate titrations, and compared ensemble population shifts (fractional

saturation) with similar solution measurements. Non-linear least-squares fitting of nMS experimental and best fit distributions of Trp_n-TRAP_n states from non-cooperative and nearest-neighbor cooperative models rule out site independence and yielded good agreement with modest nearest-neighbor cooperativity detected from temperature-dependent ITC data.

Materials and Methods:

Expression & purification of Bst TRAP: TRAP was expressed in *E. coli* BL21(DE3) cells and purified by ion exchange chromatography followed by denaturation with 6 M guanidinium hydrochloride (GdnHCl) and purification by reverse-phase HPLC to ensure removal of bound Trp, as described previously.⁴¹ Purified, lyophilized protein was dissolved in 6 M guanidinium hydrochloride (GdnHCl), 50 mM sodium phosphate, 100mM NaCl, pH 8, and refolded by a stepwise dialysis against 3 M, 1.5 M and denaturant.

NMR: Purified, refolded U-¹⁵N]-apo TRAP was divided into three 600 μ L aliquots and dialyzed into the following buffers: 50 mM NaPO₄, 100mM NaCl, pH 8.0; 100 mM ammonium acetate, pH 8.0; 100 mM ethylenediamine diacetate, pH 8.0, using 0.5 mL dialysis cassettes with a 3.5 kDa molecular weight cutoff (Thermo Slide-A-Lyzer, cat. #66333) at 4°C, with gentle stirring. The phosphate solution was pH-adjusted with 3 M NaOH.. The AmAc and EDDA solutions were pH-adjusted with 10% ammonium hydroxide. Each NMR sample contained ~1 mM TRAP protomers as measured by the Bradford assay with the Coomassie Plus Bradford reagent and bovine serum albumin as standard. Two-dimensional ¹⁵N-¹H TROSY- HSQC spectra (pulse sequence *troysf3gppsi19*) were recorded at 55°C on a Bruker Avance III HD 800 MHz spectrometer equipped with a 5 mm (TXI) cryoprobe with Z-axis gradients with 64 time points and 40 ppm spectral width in the ¹⁵N dimension.

ITC: Aliquots of 10mL of 100 μ M purified, refolded apo-TRAP were dialyzed against 1L each of three NMR buffers aforementioned for 12 hours at 4°C, and 1 mM Trp stock solutions were prepared from the dialysates. For ITC experiments, MicroCal VP-ITC isothermal titration calorimeter (Malvern Panalytical) was used. For the final concentrations, Trp and TRAP were diluted with the dialysate solutions to 600 μ M Trp in the syringe, and 60 μ M TRAP in the cell. Titrations were performed at 25°C, using an initial 3 μ L injection followed by 50 injections of 5 μ L, with a delay of 200 seconds in between injections. Data were fit to a single site model with a single apparent K_a using Origin 7.0 (OriginLab).

Native mass spectrometry: Aliquots of purified and refolded *Bst* TRAP in the phosphate buffer were exchanged twice into 200 mM ethylenediamine diacetate (EDDA; Sigma-Aldrich, cat. #420352), or 400 mM ammonium acetate (AmAc; Sigma-Aldrich, cat. #431311) using P-6 Micro Bio-Spin (BioRad) columns. The concentration of TRAP was determined by a Nanodrop 2000c spectrophotometer (Thermo Scientific™) with a monomer absorbance at 280 nm of 2980 $M^{-1}cm^{-1}$ and a mass of 8,242.6 Da.⁴² Trp stock solutions were prepared to 10 mM by dissolving in the same solutions used for the TRAP protein, and filtered with a 0.22 μ m filter. Trp stocks were diluted to 1 mM, 750 μ M and 500 μ M for native MS titration experiments. Concentrations of Trp stocks were determined with a Nanodrop 2000c spectrophotometer with an extinction coefficient at 280 nm of 5690 $M^{-1}cm^{-1}$, and a mass of 204.2 Da.⁴³ Native mass spectra were acquired on a Q Exactive EMR Plus Orbitrap (Thermo) modified with a surface-induced dissociation (SID) device and a mass selection quadrupole.⁴⁴ Data were collected at a source temperature of 175°C, nanoESI capillary voltage of 0.9–1.1 kV, in-source CID 10 V, HCD 10 V, mass range m/z 500–14,000. Flythrough (transmission) voltages were tuned to minimize activation and loss of Trp; voltages for the source DC offset, injection flatapole, inter flatapole, and bent flatapole were set at 7, 6, 5, and

5V, respectively; C-trap bias was -10V. A trap gas setting of 4 (arbitrary units) was used for recording mass spectra of samples with [TRAP] greater than 11 μM and trap gas 8 was used for the samples with [TRAP] lower than 11 μM for improved signals. Borosilicate glass capillary emitters were pulled in-house with a Sutter Flaming/Brown Micropipette puller P97. Native mass spectra were recorded for at least 1 minute at each Trp condition with 3 different emitter tips; triplicates of spectra with TRAP were acquired at 14 Trp concentrations ranging from 0 to 110 μM .

The populations of Trp_n-TRAP₁₁ species were determined from integrated peak areas after spectral deconvolution using UniDec.⁴⁵ Deconvolution was performed without smoothing, m/z range 3800 to 5700 (which includes charge states of +21 to +18 for TRAP 11-mers), mass range 91000 to 110000 Da, mass sampling of 10 Da, and peak FWHM of 2.5, manual mode, peak detection range of 3 Da, peak threshold of 0.001, and integration range of -50 to 50 Da. Peaks of TRAP were selected by manual assignment and integrated by UniDec; a m/z list of TRAP species was prepared. Populations were corrected for small amounts of Trp-loaded TRAP 12-mers by manual assignment and peak area subtraction. Fractional saturation Y at each Trp concentration was obtained from the sum of the bound Trp species at each Trp concentration:

$$\bar{Y} = \sum_{i=0}^{11} (iA_i/11)$$

where A_i is the area of mass peaks corresponding to TRAP with i bound Trp. To account for sample losses during buffer exchange, binding site concentrations were corrected by fitting fractional saturation data with an independent sites model $M + L \xrightleftharpoons{K_{D,app}} ML$ while allowing optimization of the binding site concentration M_i (i.e., 11 times the concentration of TRAP₁₁ rings) and apparent dissociation constant $K_{D,app}$. Similar results were obtained by numerical optimization of ordinary

differential equations derived from the model,⁴⁶ or analytically directly using the binding quadratic from the mass balance $\bar{Y} = (K_d + L_t + M_t - \sqrt{(K_d + L_t + M_t)^2 - 4L_tM_t})/2M_t$, where L_t is the total Trp concentration (**Figure S2**). The relative abundance of the 12 possible TRAP + Trp stoichiometries (0-11) at each concentration of TRAP and Trp ($\text{Trp}_n\text{-TRAP}_m$) were fit using *itcsimlib* as previously described¹² with slight modifications. Three statistical thermodynamic models were considered: (I) an independent sites model parametrized by an intrinsic binding free energy ΔG_i ; (II) a nearest-neighbor additive model parameterized by an intrinsic free energy change ΔG_i for binding to sites with no occupied neighbors and a cooperativity term ΔG_m that is doubled when both neighboring sites are occupied; and (III) a non-additive model parametrized by ΔG_i , and cooperativity terms ΔG_{m1} and ΔG_{m2} which correspond to the effects of having one or two occupied neighbors.¹² Suitable binding polynomials are constructed in an automated manner by *itcsimlib* by iterating over all possible possible $\text{Trp}_n\text{-TRAP}_m$ configurations ($2^{11} = 2048$), and statistical thermodynamic probabilities are computed at each ligand and binding site concentration; compared to fitting ITC data, populations are used directly, with zero binding enthalpies. Free energy terms of the model were optimized by numerical minimization of the reduced chi-square test value between the experimental and simulated populations using an estimated variance of 0.05%.

RESULTS AND DISCUSSION

TRAP structure is unperturbed by MS-compatible electrolyte solutions

To be useful for measuring binding thermodynamics, the conditions used for recording native mass spectra should not perturb the quaternary structure and populations of free and bound states, and the detected ion counts should mirror the abundance of the species present in solution. We used two-dimensional NMR spectroscopy to examine the effect of MS-compatible solutions on

the solution structure of TRAP. Two-dimensional ^{15}N - ^1H TROSY-HSQC spectra of TRAP were recorded in both typical and nMS-compatible pH 8 solutions: 1) 50 mM sodium phosphate, 100 mM NaCl, 2) 100 mM ammonium acetate (AmAc), and 3) 100 mM ethylenediamine diacetate (EDDA) (**Figure 2, top**). The 11-fold symmetry of the 91 kDa Trp-free TRAP oligomer results in spectra that feature a single set of resonances for each of the amino acids in the 74-residue protein. NMR spectra from each of the solutions exhibited indistinguishable chemical shifts and linewidths for nearly all signals observed in the spectra; only three resonances exhibit chemical shift perturbations (CSPs) greater than 0.02 ppm. While there is evidence for more native-like structure of lower charge ions sprayed from EDDA versus AmAc,^{38,39,47,48} there were no CSPs > 0.02 ppm between those conditions, indicating that the solution structure of TRAP in those buffers is indistinguishable. Likewise, the amide spectra of TRAP in the presence of excess Trp were similarly unperturbed by the choice of electrolyte solution (data not shown). As amide chemical shifts are highly sensitive to changes in local electronic environment, we conclude that the protein structure is not significantly altered by the solution components investigated.

TRAP binds Trp with comparable thermodynamics in MS-compatible electrolyte solutions

We used isothermal titration calorimetry (ITC) to test whether use of MS-compatible solutions might alter Trp binding thermodynamics. Identical TRAP samples were dialyzed into each of the solutions used in NMR experiments: phosphate, AmAc, and EDDA (pH 8) and loaded into the sample cell, while crystalline Trp was dissolved into the corresponding buffers, loaded into the syringe, and titration experiments were performed at 25°C (**Figure 2, bottom**). Although Trp exhibits weak cooperativity in binding to TRAP (as shown below and previously noted in temperature-dependent studies),¹² thermograms from each solution were reasonably well described by a single-site model. Fitting integrated enthalpies yielded similar binding enthalpies (ΔH -14.51

$\pm 0.02 \text{ kcal mol}^{-1}$, $-16.00 \pm 0.05 \text{ kcal mol}^{-1}$, and $-16.92 \pm 0.08 \text{ kcal mol}^{-1}$) and affinities ($K_{d,app}$ $0.115 \pm 0.003 \mu\text{M}$, $0.173 \pm 0.014 \mu\text{M}$ and $0.183 \pm 0.010 \mu\text{M}$) in phosphate, AmAc and EDDA solutions, respectively. These affinity differences are within thermal energy ($RT = 590 \text{ cal/mol}$ at 25°C), and thus we conclude that under these conditions the thermodynamics of the Trp-TRAP interaction are not significantly perturbed by the MS-compatible AmAc and EDDA solutions in comparison to use of phosphate buffer.

Choice of electrolyte solution does not significantly affect measurement of Trp-TRAP binding by native MS

Before proceeding to quantitatively interpret populations of $\text{Trp}_n\text{-TRAP}_n$ states in a titration, we examined the possibility that the choice of solution might affect the ion counts in the gas phase. Previous nMS experiments with TRAP have shown that Trp can remain bound to TRAP when the ligand is in excess, and though populations of states were not interpreted quantitatively, different gas-phase structures were inferred from ion mobility experiments.^{38,39} To determine the effect of electrolyte solution on MS-detected charge states and populations of ions corresponding to TRAP complexes with varying numbers of bound Trp, we recorded nMS spectra of TRAP in the absence and presence of Trp from both AmAc and EDDA solutions (**Figure 3**). Whether sprayed from AmAc or EDDA, spectra in the absence of Trp were dominated by ions corresponding to multiply charged intact undecamers (90,665.96 Da). In the EDDA solution (pH 8), the dominant charge state distribution (CSD) includes 20+ and 19+ charge states, while in AmAc (pH 7) we observed a distribution of higher charge states, with dominant 23+ and 22+ charge states; this charge state difference is consistent with previous findings.^{38,39,47,48} In the presence of roughly $\frac{1}{2}$ equivalents of Trp per binding site (~ 5.5 equivalents per TRAP_n ring), we observe for each charge state a series of well-separated peaks that correspond to the mass of TRAP_n with varying numbers of bound Trp

(from 0 to 11). In either AmAc or EDDA, spectra yielded narrow charge state distributions and well-resolved peaks corresponding to similar distributions of Trp₀₋₁₁-TRAP₁₁ states. Well-resolved peaks of the Trp_n-TRAP₁₁ states yielded similar quantification of populations from either intensities or integration of peak areas, consistent with the fact that peak widths and shapes don't vary significantly across the measured m/z range.

Native MS allows quantifying populations of Trp_n-TRAP₁₁ states

Solution NMR and ITC experiments showed no significant difference in structure or thermodynamics between phosphate buffer and AmAc and EDDA solutions, so we proceeded with native MS experiments to measure populations of Trp_n-TRAP₁₁ states sprayed from 200 mM EDDA solutions (pH 8) after pre-mixing a range of TRAP concentrations with a range of Trp concentrations from 0 to ~2-fold excess relative to the number of binding sites. Over the course of a typical titration (**Figure 4**), a clear shift in populations is observed, starting from apo-TRAP (Trp₀-TRAP₁₁, 90,657 Da; top spectrum in **Figure 4**) to holo-TRAP (Trp₁₁-TRAP₁₁, 92,930 Da; bottom spectrum). Throughout most of the titration series in EDDA, spectra are dominated by signals from the 20+ and 19+ charge states. For this series, with ~5 μ M binding sites, signals from fully bound holo-TRAP (Trp₁₁-TRAP₁₁) become the dominant feature of the spectrum above 7 μ M Trp (~ 1.4 equivalents), indicating a c value ($c = [\text{sites}]/K_d = [5.46 \mu\text{M}/0.5 \mu\text{M}]$), not far above 1 (see below for $K_{d,app}$).¹⁷ With a low c value, there is a sub-stoichiometric binding of Trp to TRAP under these conditions.

Populations of Trp_n-TRAP₁₁ species at each Trp concentration were obtained by integration of deconvoluted spectra (**Figure S1**). The low extinction coefficient of TRAP ($\epsilon_{280} 2980 \text{ M}^{-1} \text{ cm}^{-1}$)¹², and additional handling steps while performing electrospray experiments made it difficult to precisely control protein concentration. Protein concentrations were corrected by non-linear least-squares

fitting of the summed bound fraction \bar{Y} with an independent sites model (**Fig. S2**). Fits yielded corrected protein concentrations with % changes ranging from 15.8% to 54.7% from initial TRAP concentrations (**Table S1**), and apparent dissociation constants $K_{d,app}$ of $\sim 0.5 \mu\text{M}$ for each Trp binding site (**Figure S2, Table S1**). Trp concentrations ($\epsilon_{280} 5690 \text{ M}^{-1}\text{cm}^{-1}$)⁴³ were taken to be accurate. Importantly, the resulting populations of $\text{Trp}_n\text{-TRAP}_{11}$ species allows separate quantitation of TRAP_{11} species with different numbers of bound Trp, whereas this information is difficult to obtain from conventional approaches such as ITC which provide only a measure of overall fractional saturation (**Figure S1**).

Cooperative Trp binding to TRAP_{11} is evident from population distributions

Independent quantification of $\text{Trp}_n\text{-TRAP}_{11}$ populations clearly distinguishes independent and cooperative ligand binding. Although the unidimensional metric of fractional saturation \bar{Y} could be readily fit by a binding polynomial with a single equilibrium constant (**Fig. S2, Table S1**), we first tested whether the experimentally determined $\text{Trp}_n\text{-TRAP}_{11}$ populations (**Fig. 5, left**, 19+ charge state used for illustration) could be explained by a model with 11 independent sites (i.e., a binomial distribution), by comparing experimental mass spectra with those simulated from populations obtained by best fit to an independent sites model (**Figure 5, middle**). Simulated spectra from the independent sites model were in poor agreement with the experimental data, featuring a generally narrower distribution across the titration range. On the other hand, fitting the experimental populations with binding polynomials generated from a nearest-neighbor model produced broader distributions of $\text{Trp}_n\text{-TRAP}_{11}$ states and generally good fits to the experimental data (**Fig. 5, right**). This binding model is parametrized with an intrinsic affinity of isolated sites for binding to a Trp ligand, ΔG_{\circ} , plus terms for how this affinity is altered by the occupancy of one or two neighboring sites, $\Delta G_{\circ,1}$, $\Delta G_{\circ,2}$ (**Figure 1**). The stark difference in population distributions

obtained experimentally, in comparison to those from the independent and nearest-neighbor models illustrates the advantage of being able to independently measure different components of the partition function, and highlights the tremendous advantage of using native MS to monitor ligand binding to proteins with multiple binding sites.

Populations derived from native MS spectra of each of the six independent titration experiments were well described by the nearest-neighbor model, yielding three free energy terms ΔG_i , ΔG_{oc} , ΔG_{oo} (**Figure 1**).¹² After fitting to this *non-additive* nearest-neighbor model, we found that the best-fit values of ΔG_{oo} were within error of twice ΔG_{oc} , indicating that an *additive* nearest-neighbor model with only two parameters was appropriate, with free energies for binding to isolated sites ΔG_i , one occupied neighbor $\Delta G_i + \Delta G_b$, and two occupied neighbors $\Delta G_i + 2\Delta G_b$. For the six independent experiments, best fit mean and standard deviations were ΔG_i -6.86 ± 0.50 kcal mol⁻¹, and ΔG_b -0.56 ± 0.09 kcal mol⁻¹, yielding free energies for binding to sites with 0, 1 or 2 occupied neighbors of -6.86 ± 0.50 , -7.41 ± 0.43 and -7.93 ± 0.38 kcal mol⁻¹, respectively. These binding free energies correspond to microscopic dissociation constants for sites with 0, 1 or 2 bound neighbors, of 12.29, 4.68 and 1.82 μ M, respectively. These parameters are consistent with the weak positive cooperativity previously determined from nearest-neighbor modeling of ITC data.¹²

Sources of Error

Although population distributions throughout the six independent titrations were highly reproducible, and the analysis yielded a narrow range of best-fit thermodynamic parameters, we observed three sources of variability in the data. First, as mentioned above, was difficulty in precisely defining the concentration of binding sites (i.e., TRAP) in the experiments. This usually resulted in titration series that seemed to saturate at somewhat lower than expected Trp concentrations. After correcting the TRAP concentration for each series by mass balance analysis,

saturation points and population distributions converged. Second, best-fit binding free energies were somewhat correlated with TRAP concentration, exhibiting increasing affinity with decreasing protein concentration (**Figure S3, Table S2**). Although not definitive, this observation may be consistent with formation of small populations of TRAP 12-mers with altered affinity for Trp. Indeed, in some of the titrations we observed low abundance signals corresponding to TRAP₁₂ (MW 101,363 Da with normalized intensity as high as 10.5% compared to the 11-mer); although uncommon, small populations of TRAP 12-mers have been observed in mass spectrometry experiments⁸ as well as a few solution experiments,^{49,50} and in crystals.³³ In addition, we observed signals corresponding to trace dimers of TRAP₁₁ (“double-donuts”), in agreement with previous solution experiments.^{51,52} However, the signals from this species were too low in abundance for reliable quantitation and thus their populations were considered too low to be included in the analysis. Third, upon closer analysis we observed some charge state-dependent variability in abundance of Trp_n-TRAP₁₁ signals in the nMS spectra, complicated by different relative abundances and signal/noise for different charge states (**Figure S4**); separate analysis of Trp_n-TRAP₁₁ populations for different charge states thus resulted in slightly different best fit thermodynamic parameters (**Table S3**). By comparison, we observed decreased charge state dependence in AmAc data (**Figure S5, Table S4**). Although this phenomenon merits further investigation, this charge-state dependent effect resulted in generally less variability than observed between replicates (free energy difference of 0.083 kcal mol⁻¹ in EDDA, compared to a standard deviation of 0.502 kcal mol⁻¹ between replicates), and positive nearest-neighbor cooperativity was required to produce reasonable fits to each dataset. *Overall, the titration series yielded reproducible shifts in Trp_n-TRAP₁₁ populations consistent with the nearest-neighbor cooperativity model and inconsistent with*

*non-cooperative independent binding to the 11 sites, as found previously by analysis of temperature-dependent ITC data.*¹²

Conclusions

A requisite for describing an allosteric mechanism is an accurate description of the microscopic thermodynamic parameters that distinguish ligand binding events. Traditional solution-based methods for obtaining thermodynamic parameters by fitting experimentally determined observables to binding models are generally under determined when the number of binding sites and parameters expand, and loss of proportionality between the observable and the populations further obfuscates mechanism. Because the mass of a macromolecule-ligand complex uniquely defines the number of bound ligands, native mass spectrometry has the potential to probe the ligand-protein partition function at a resolution difficult to achieve with other techniques. In the case of TRAP, direct measurement of Trp_n-TRAP_n populations by nMS enabled detection and quantification of cooperativity without the need to perform titrations over a range of concentrations and temperature ranges to resolve distinct thermodynamic binding modes.¹² The approach requires the capability of resolving masses with different numbers of bound ligands, that the MS-compatible solutions not perturb the underlying thermodynamics (populations of liganded states), and that the detected ions accurately reflect populations present in solution. Moreover, real insight requires development and testing of accurate mechanistic models with the appropriate microscopic thermodynamic constants. While not all of these requirements are likely to be met for all cases, we expect that nMS will transform how we approach quantification and understanding of allosteric mechanisms in the plethora of important, homo-oligomeric proteins that function via cooperative ligand binding.

Supporting Information.

The following files are available free of charge.

Supplemental Figures and Tables. (PDF)

Accession Codes

UniProt: Q9X6J6

Abbreviations

TRAP, trp RNA-binding attenuation protein; nMS, native mass spectrometry; NMR, nuclear magnetic resonance; ITC, isothermal titration calorimetry; AmAc, ammonium acetate; EDDA, ethylenediamine diacetate

Author Contributions

P.G. provided the protein for the experiments which was further purified by M.L.H. For *itcsimlib*, E.C.I. created scripts for fitting nMS data. M.L.H. performed all of the biochemical experiments, data analyses and interpretation with input from M.P.F. and V.H.W. M.L.H. prepared the initial drafts of the figures and text, which were edited and finalized by M.P.F. and V.H.W. with input from all other co-authors. M.P.F. and V.H.W. secured funding to support this project and provided intellectual support for all aspects of the work. All authors have given approval to the final version of the manuscript.

Funding

This work was funded by NIH grant R01 GM077234 (Foster), P41 GM128577 (Wysocki), and T32 GM086252 (Holmquist).

Acknowledgements

We thank the Gollnick lab members (especially Skylar Kelly) for protein overexpression and purification, the Wysocki lab members for sharing their MS expertise, and the Foster lab, especially Weicheng Li, Cameron Jamshidi, and Dr. Deepak Kumar for their input and assistance with TRAP. We thank Drs. Alex Hansen and Chunhua Yuan of Ohio State University's Campus Chemical Instrumentation Center for their assistance with the NMR instruments. We thank the Student Life Disabilities Services (SLDS) at the Ohio State University for the interpreting services provided by their American Sign Language Interpreters.

Figures & Legends

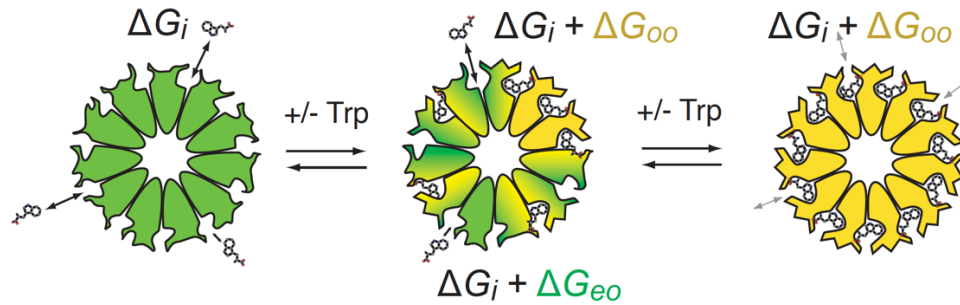


Figure 1: Tryptophan (Trp) binding to the homo-undecameric (11-mer) ring protein TRAP, and nearest-neighbor (NN) microscopic free energy terms to describe cooperative Trp binding. Tryptophan binds to apo TRAP (green) in identical sites located between adjacent protomers, resulting in local conformational changes that activate (yellow) it for specific binding to the *trp* leader RNA. The NN model posits an intrinsic free energy ΔG_i for binding to sites with no occupied neighbors, whereas binding to sites with one or two occupied neighbors incur additional free energy terms ΔG_{eo} and $2\Delta G_{oo}$, respectively.

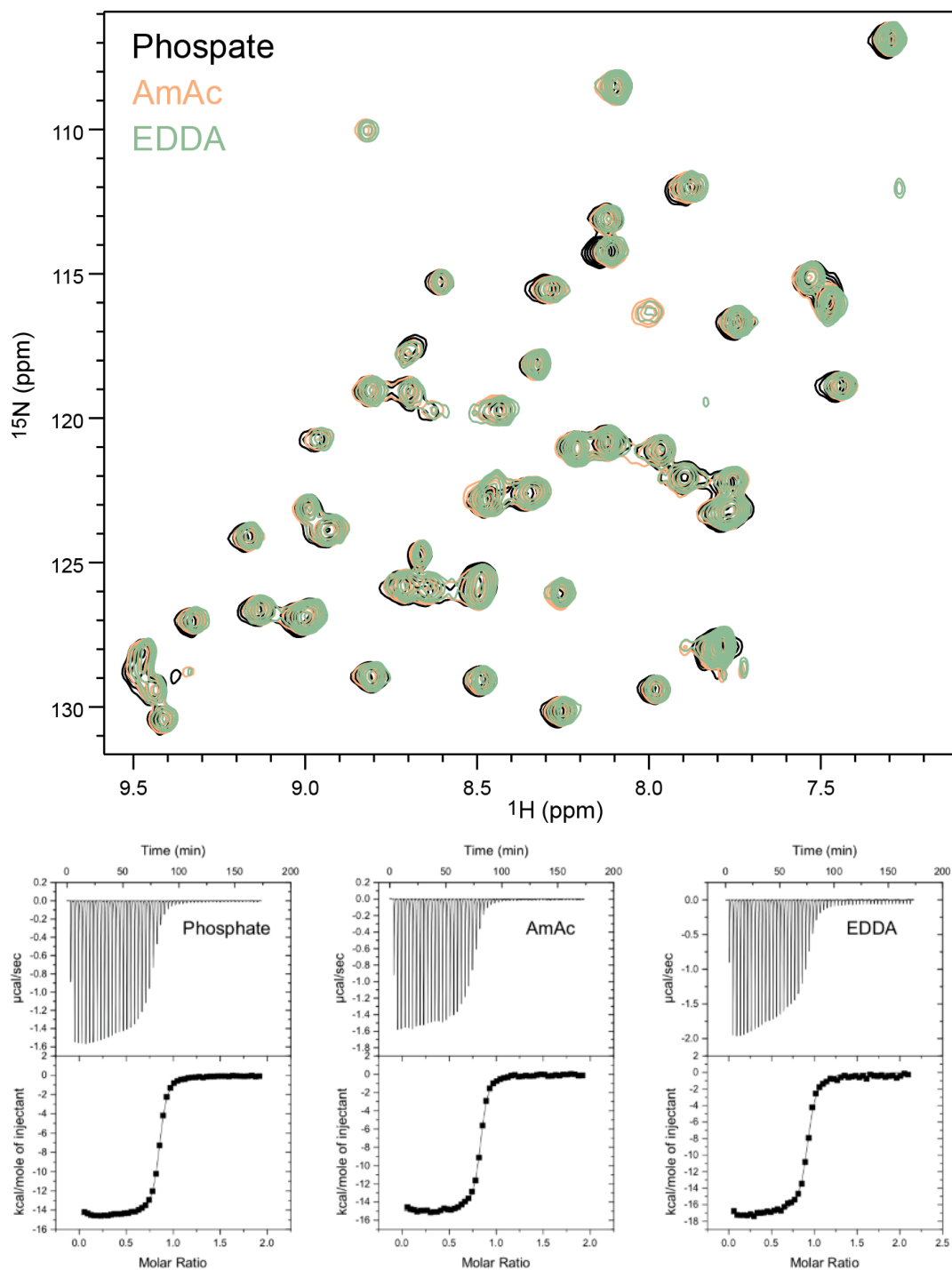


Figure 2: Solutions compatible with native mass spectrometry (nMS) do not significantly alter the structure of TRAP or its Trp binding thermodynamics. (Top) Two-dimensional ^{15}N - ^1H TROSY-HSQC spectra of TRAP recorded at 800 MHz in typical (50 mM sodium phosphate, 100 mM NaCl, pH 8.0), or nMS-compatible solutions (100 mM ammonium acetate (AmAc), pH 8.0; 100

mM ethylene diamine diacetate (EDDA), pH 8.0); most resonances superpose within < 0.02 ppm. (Bottom) Isothermal titration calorimetry (ITC) yields similar thermograms in phosphate and nMS-compatible solutions. ITC titrations were performed at 25°C with 600 μM Trp titrated into 60 μM TRAP protomers (5.5 μM rings) in (i) 50 mM sodium phosphate, 100 mM NaCl, pH 8.0, (ii) 100 mM ammonium acetate, pH 8.0, and (iii) 100 mM ethylenediamine diacetate, pH 8.0. Apparent dissociation constants fitted to a one-site model were $0.115 \pm 0.003 \mu\text{M}$, $0.173 \pm 0.014 \mu\text{M}$, and $0.183 \pm 0.010 \mu\text{M}$ in phosphate, AmAc and EDDA, respectively.

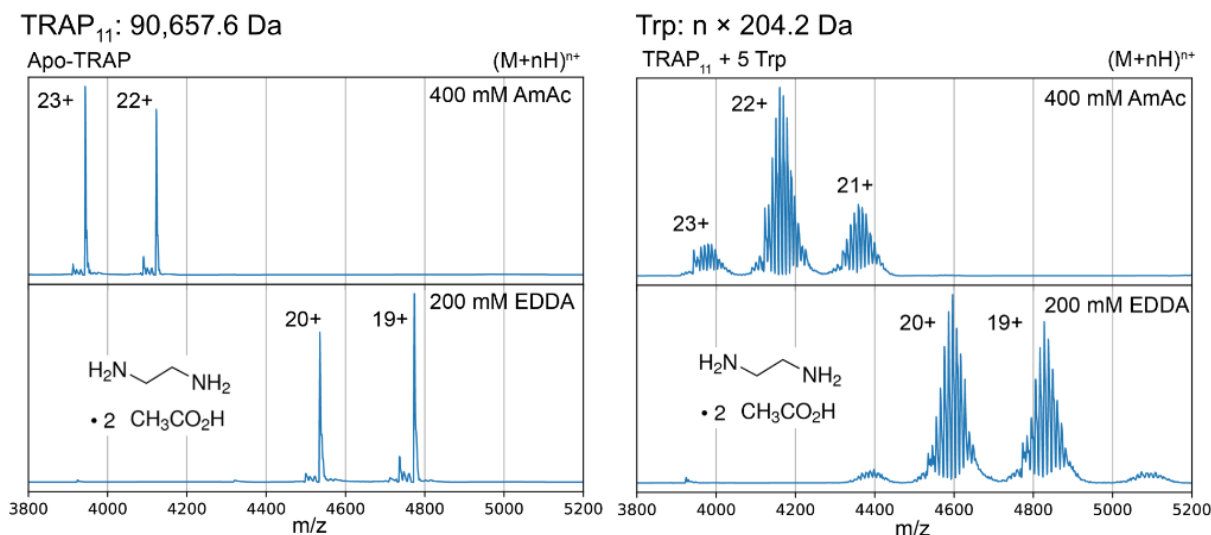


Figure 3: Nano-ESI spectra of TRAP exhibit native-like features, including narrow charge states distributions, an oligomeric state corresponding to TRAP₁₁-mer, and non-covalent ligand interactions. Mass spectra were obtained for 5 μM *Bst* TRAP₁₁ in 400 mM AmAc and 200 mM EDDA. (Left) Trp-free apo-TRAP₁₁ exhibits dominant 23+ and 22+ charge states when sprayed from 400 mM AmAc, and 20+ and 19+ charge states from 200 mM EDDA. (Right) TRAP₁₁ in the presence of 25 μM Trp retain similar populations of Trp_n-TRAP₁₁ states, with slightly higher charge states (23+ to 21+) in AmAc than in EDDA (21+ to 18+).

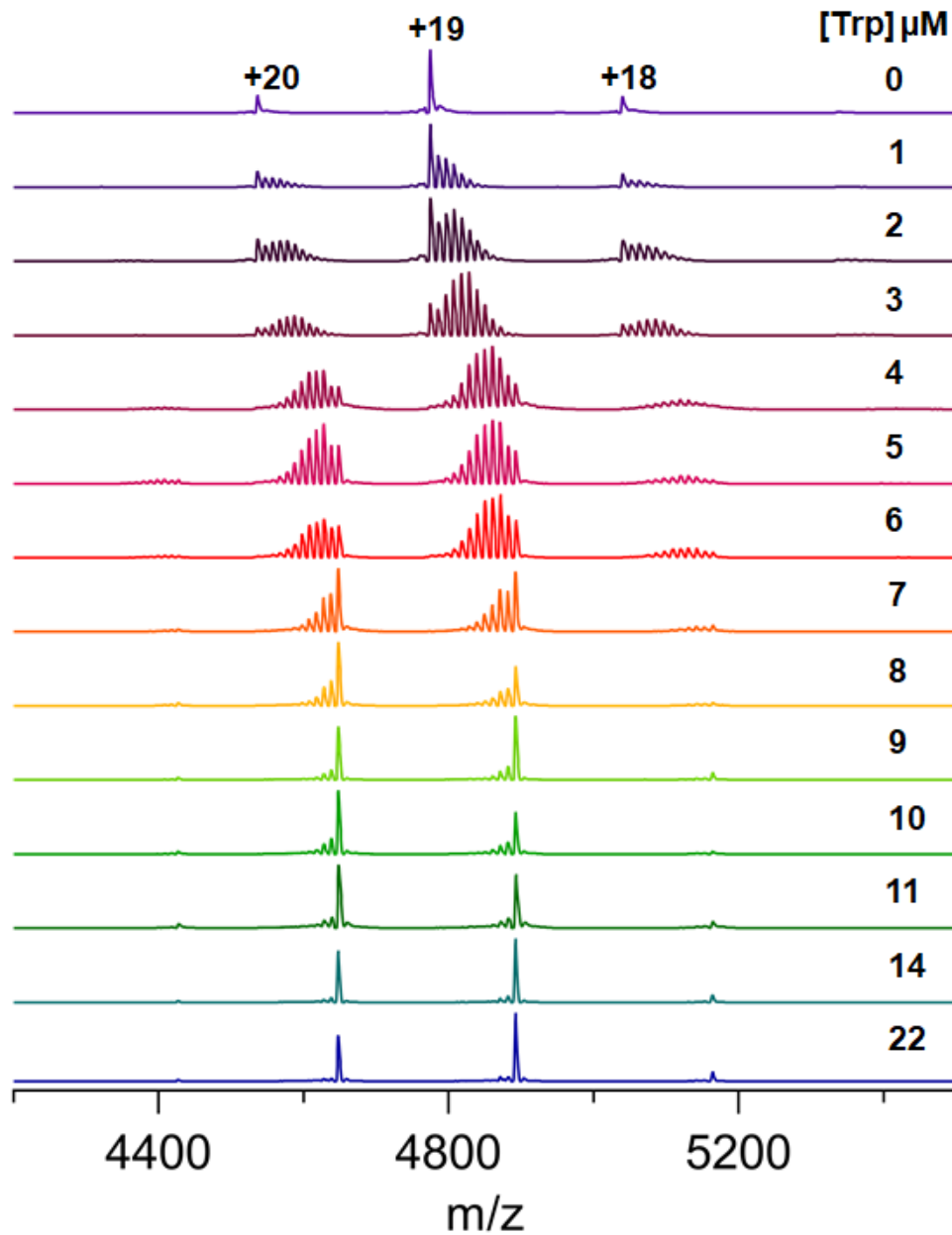


Figure 4: Native MS reveals populations of Trp_n-TRAP₁₁ states via a titration. 0.5 μM TRAP₁₁ in 200 mM EDDA was titrated with 1-22 μM Trp, yielding prominent ions in 20+ to 18+ charge states, with 0-11 bound Trp. At 0 μM Trp, only the apo form of TRAP₁₁ is observed, whereas at high Trp concentrations and higher the Trp_n-TRAP₁₁ signals predominate.

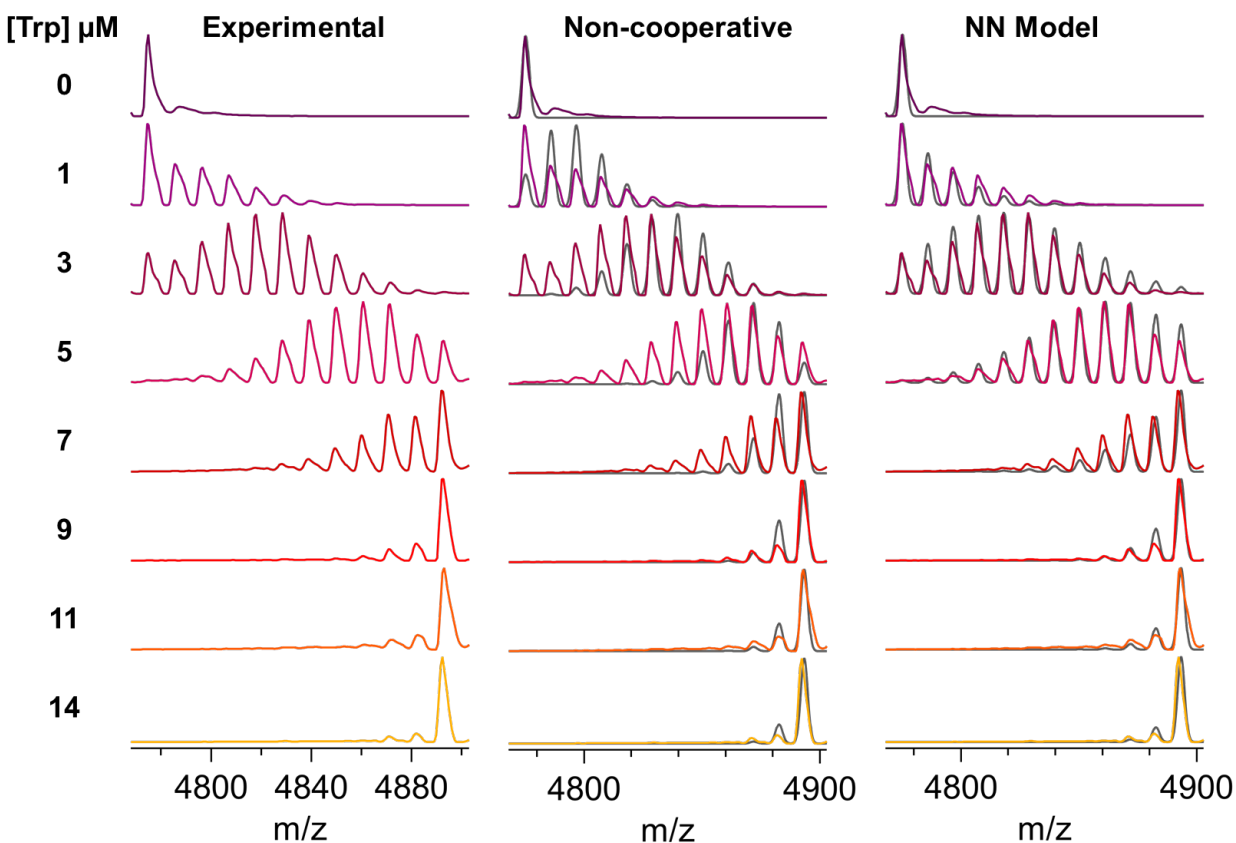


Figure 5: Population distribution of $\text{Trp}_n\text{-TRAP}_{11}$ states reveals homotropic cooperativity in Trp binding to TRAP_{11} . Populations of $\text{Trp}_n\text{-TRAP}_{11}$ states were fit with a binding polynomial derived from either an independent sites model, or a nearest-neighbor cooperative model. Left, experimental spectra for the 19+ charge state for 1 μM TRAP_{11} recorded after incubating with the indicated concentration of Trp. Middle and right, the experimental data were overlaid with spectra simulated using populations computed from best fits to the independent sites model (middle), or the nearest neighbor cooperative model (right). The experimental population distributions are poorly described by the independent sites model, whereas the NN model generates excellent fits. Best fit parameters for the NN model were ΔG_i of -6.86 ± 0.50 kcal mol⁻¹ and ΔG_b of -0.56 ± 0.09 kcal mol⁻¹ (Table S1).

References

1. Goodsell, D.S. and Olson, A.J. Structural symmetry and protein function. *Annu Rev Biophys Biomol Struct*, 2000. 29: p. 105-53.
2. Andre, I., Strauss, C.E., Kaplan, D.B., Bradley, P., and Baker, D. Emergence of symmetry in homooligomeric biological assemblies. *Proc Natl Acad Sci U S A*, 2008. 105(42): p. 16148-52.
3. Bergendahl, L.T. and Marsh, J.A. Functional determinants of protein assembly into homomeric complexes. *Sci Rep*, 2017. 7(1): p. 4932.
4. Olivares, A.O., Baker, T.A., and Sauer, R.T. Mechanistic insights into bacterial AAA+ proteases and protein-remodelling machines. *Nat Rev Microbiol*, 2016. 14(1): p. 33-44.
5. Skjaerven, L., Cuellar, J., Martinez, A., and Valpuesta, J.M. Dynamics, flexibility, and allostery in molecular chaperonins. *FEBS Lett*, 2015. 589(19 Pt A): p. 2522-32.
6. Cui, Q. and Karplus, M. Allostery and cooperativity revisited. *Protein Sci*, 2008. 17(8): p. 1295-307.
7. Holt, J.M. and Ackers, G.K. The Hill coefficient: inadequate resolution of cooperativity in human hemoglobin. *Methods Enzymol*, 2009. 455: p. 193-212.
8. Hilser, V.J., Wrabl, J.O., and Motlagh, H.N. Structural and energetic basis of allostery. *Annu Rev Biophys*, 2012. 41: p. 585-609.
9. Changeux, J.P. Allostery and the Monod-Wyman-Changeux model after 50 years. *Annu Rev Biophys*, 2012. 41: p. 103-33.

10. Gruber, R. and Horovitz, A. Unpicking allosteric mechanisms of homo-oligomeric proteins by determining their successive ligand binding constants. *Philos Trans R Soc Lond B Biol Sci*, 2018. 373(1749).
11. Wodak, S.J., Paci, E., Dokholyan, N.V., Berezovsky, I.N., Horovitz, A., Li, J., Hilser, V.J., Bahar, I., Karanicolas, J., Stock, G., Hamm, P., Stote, R.H., Eberhardt, J., Chebaro, Y., Dejaegere, A., Cecchini, M., Changeux, J.P., Bolhuis, P.G., Vreede, J., Faccioli, P., Orioli, S., Ravasio, R., Yan, L., Brito, C., Wyart, M., Gkeka, P., Rivalta, I., Palermo, G., McCammon, J.A., Panecka-Hofman, J., Wade, R.C., Di Pizio, A., Niv, M.Y., Nussinov, R., Tsai, C.J., Jang, H., Padhorny, D., Kozakov, D., and McLeish, T. Allostery in Its Many Disguises: From Theory to Applications. *Structure*, 2019. 27(4): p. 566-578.
12. Ihms, E.C., Kleckner, I.R., Gollnick, P., and Foster, M.P. Mechanistic Models Fit to Variable Temperature Calorimetric Data Provide Insights into Cooperativity. *Biophys J*, 2017. 112(7): p. 1328-1338.
13. Brown, A. Analysis of cooperativity by isothermal titration calorimetry. *Int J Mol Sci*, 2009. 10(8): p. 3457-77.
14. Vega, S., Abian, O., and Velazquez-Campoy, A. A unified framework based on the binding polynomial for characterizing biological systems by isothermal titration calorimetry. *Methods*, 2015. 76: p. 99-115.
15. Zhao, H., Piszczek, G., and Schuck, P. SEDPHAT--a platform for global ITC analysis and global multi-method analysis of molecular interactions. *Methods*, 2015. 76: p. 137-148.

16. Freiburger, L.A., Auclair, K., and Mittermaier, A.K. Elucidating protein binding mechanisms by variable-c ITC. *Chembiochem*, 2009. 10(18): p. 2871-3.
17. Wiseman, T., Williston, S., Brandts, J.F., and Lin, L.N. Rapid measurement of binding constants and heats of binding using a new titration calorimeter. *Anal Biochem*, 1989. 179(1): p. 131-7.
18. Heck, A.J. Native mass spectrometry: a bridge between interactomics and structural biology. *Nat Methods*, 2008. 5(11): p. 927-33.
19. Marcoux, J. and Robinson, C.V. Twenty years of gas phase structural biology. *Structure*, 2013. 21(9): p. 1541-50.
20. Busch, F., VanAernum, Z.L., Ju, Y., Yan, J., Gilbert, J.D., Quintyn, R.S., Bern, M., and Wysocki, V.H. Localization of Protein Complex Bound Ligands by Surface-Induced Dissociation High-Resolution Mass Spectrometry. *Anal Chem*, 2018. 90(21): p. 12796-12801.
21. Dyachenko, A., Gruber, R., Shimon, L., Horovitz, A., and Sharon, M. Allosteric mechanisms can be distinguished using structural mass spectrometry. *Proc Natl Acad Sci U S A*, 2013. 110(18): p. 7235-9.
22. Cong, X., Liu, Y., Liu, W., Liang, X., Russell, D.H., and Laganowsky, A. Determining Membrane Protein-Lipid Binding Thermodynamics Using Native Mass Spectrometry. *J Am Chem Soc*, 2016. 138(13): p. 4346-9.
23. Hernandez, H. and Robinson, C.V. Determining the stoichiometry and interactions of macromolecular assemblies from mass spectrometry. *Nat Protoc*, 2007. 2(3): p. 715-26.

24. Susa, A.C., Xia, Z., Tang, H.Y.H., Tainer, J.A., and Williams, E.R. Charging of Proteins in Native Mass Spectrometry. *J Am Soc Mass Spectrom*, 2017. 28(2): p. 332-340.
25. Susa, A.C., Xia, Z., and Williams, E.R. Native Mass Spectrometry from Common Buffers with Salts That Mimic the Extracellular Environment. *Angew Chem Int Ed Engl*, 2017. 56(27): p. 7912-7915.
26. Chait, B.T., Cadene, M., Olinares, P.D., Rout, M.P., and Shi, Y. Revealing Higher Order Protein Structure Using Mass Spectrometry. *J Am Soc Mass Spectrom*, 2016. 27(6): p. 952-65.
27. Ma, X., Zhou, M., and Wysocki, V.H. Surface induced dissociation yields quaternary substructure of refractory noncovalent phosphorylase B and glutamate dehydrogenase complexes. *J Am Soc Mass Spectrom*, 2014. 25(3): p. 368-79.
28. Zhou, M. and Wysocki, V.H. Surface induced dissociation: dissecting noncovalent protein complexes in the gas phase. *Acc Chem Res*, 2014. 47(4): p. 1010-8.
29. Gollnick, P., Babitzke, P., Antson, A., and Yanofsky, C. Complexity in regulation of tryptophan biosynthesis in *Bacillus subtilis*. *Annu Rev Genet*, 2005. 39: p. 47-68.
30. McElroy, C.A., Manfredo, A., Gollnick, P., and Foster, M.P. Thermodynamics of tryptophan-mediated activation of the trp RNA-binding attenuation protein. *Biochemistry*, 2006. 45(25): p. 7844-53.
31. Antson, A.A., Otridge, J., Brzozowski, A.M., Dodson, E.J., Dodson, G.G., Wilson, K.S., Smith, T.M., Yang, M., Kurecki, T., and Gollnick, P. The structure of trp RNA-binding attenuation protein. *Nature*, 1995. 374(6524): p. 693-700.

32. Saroff, H.A. and Keifer, J.E. Analysis of the binding of ligands to large numbers of sites: the binding of tryptophan to the 11 sites of the trp RNA-binding attenuation protein. *Anal. Biochem.*, 1997. 247: p. 138-142.
33. Heddle, J.G., Okajima, T., Scott, D.J., Akashi, S., Park, S.Y., and Tame, J.R. Dynamic allostery in the ring protein TRAP. *J Mol Biol*, 2007. 371(1): p. 154-67.
34. Chen, X., Antson, A.A., Yang, M., Li, P., Baumann, C., Dodson, E.J., Dodson, G.G., and Gollnick, P. Regulatory features of the trp operon and the crystal structure of the trp RNA-binding attenuation protein from *Bacillus stearothermophilus*. *J Mol Biol*, 1999. 289(4): p. 1003-16.
35. Li, P.T. and Gollnick, P. Using hetero-11-mers composed of wild type and mutant subunits to study tryptophan binding to TRAP and its role in activating RNA binding. *J Biol Chem*, 2002. 277(38): p. 35567-73.
36. Yang, M., Chen, X., Militello, K., Hoffman, R., Fernandez, B., Baumann, C., and Gollnick, P. Alanine-scanning mutagenesis of *Bacillus subtilis* trp RNA-binding attenuation protein (TRAP) reveals residues involved in tryptophan binding and RNA binding. *J Mol Biol*, 1997. 270(5): p. 696-710.
37. Otridge, J. and Gollnick, P. MtrB from *Bacillus subtilis* binds specifically to trp leader RNA in a tryptophan-dependent manner. *Proc Natl Acad Sci U S A*, 1993. 90(1): p. 128-32.
38. Ruotolo, B.T., Giles, K., Campuzano, I., Sandercock, A.M., Bateman, R.H., and Robinson, C.V. Evidence for macromolecular protein rings in the absence of bulk water. *Science*, 2005. 310(5754): p. 1658-61.

39. McCammon, M.G., Hernandez, H., Sobott, F., and Robinson, C.V. Tandem mass spectrometry defines the stoichiometry and quaternary structural arrangement of tryptophan molecules in the multiprotein complex TRAP. *J Am Chem Soc*, 2004. 126(19): p. 5950-1.
40. Akashi, S., Watanabe, M., Heddle, J.G., Unzai, S., Park, S.Y., and Tame, J.R. RNA and protein complexes of trp RNA-binding attenuation protein characterized by mass spectrometry. *Anal Chem*, 2009. 81(6): p. 2218-26.
41. McElroy, C., Manfredo, A., Wendt, A., Gollnick, P., and Foster, M. TROSY-NMR studies of the 91kDa TRAP protein reveal allosteric control of a gene regulatory protein by ligand-altered flexibility. *J Mol Biol*, 2002. 323(3): p. 463-73.
42. Kleckner, I.R., McElroy, C.A., Kuzmic, P., Gollnick, P., and Foster, M.P. Homotropic cooperativity from the activation pathway of the allosteric ligand-responsive regulatory trp RNA-binding attenuation protein. *Biochemistry*, 2013. 52(49): p. 8855-65.
43. Edelhoch, H. Spectroscopic determination of tryptophan and tyrosine in proteins. *Biochemistry*, 1967. 6(7): p. 1948-54.
44. VanAernum, Z.L., Gilbert, J.D., Belov, M.E., Makarov, A.A., Horning, S.R., and Wysocki, V.H. Surface-Induced Dissociation of Noncovalent Protein Complexes in an Extended Mass Range Orbitrap Mass Spectrometer. *Anal Chem*, 2019. 91(5): p. 3611-3618.
45. Marty, M.T., Baldwin, A.J., Marklund, E.G., Hochberg, G.K., Benesch, J.L., and Robinson, C.V. Bayesian deconvolution of mass and ion mobility spectra: from binary interactions to polydisperse ensembles. *Anal Chem*, 2015. 87(8): p. 4370-6.

46. Kuzmic, P. Program DYNAFIT for the analysis of enzyme kinetic data: application to HIV proteinase. *Anal Biochem*, 1996. 237(2): p. 260-73.
47. Ruotolo, B.T., Benesch, J.L., Sandercock, A.M., Hyung, S.J., and Robinson, C.V. Ion mobility-mass spectrometry analysis of large protein complexes. *Nat Protoc*, 2008. 3(7): p. 1139-52.
48. Konermann, L., Metwally, H., Duez, Q., and Peters, I. Charging and supercharging of proteins for mass spectrometry: recent insights into the mechanisms of electrospray ionization. *Analyst*, 2019. 144(21): p. 6157-6171.
49. Bayfield, O.W., Chen, C.S., Patterson, A.R., Luan, W., Smits, C., Gollnick, P., and Antson, A.A. Trp RNA-binding attenuation protein: modifying symmetry and stability of a circular oligomer. *PLoS One*, 2012. 7(9): p. e44309.
50. Heddle, J.G., Yokoyama, T., Yamashita, I., Park, S.Y., and Tame, J.R. Rounding up: Engineering 12-membered rings from the cyclic 11-mer TRAP. *Structure*, 2006. 14(5): p. 925-33.
51. Ihms, E.C., Zhou, M., Zhang, Y., Kleckner, I.R., McElroy, C.A., Wysocki, V.H., Gollnick, P., and Foster, M.P. Gene regulation by substoichiometric heterocomplex formation of undecameric TRAP and trimeric anti-TRAP. *Proc Natl Acad Sci U S A*, 2014. 111(9): p. 3442-7.
52. Snyder, D., Lary, J., Chen, Y., Gollnick, P., and Cole, J.L. Interaction of the trp RNA-binding attenuation protein (TRAP) with anti-TRAP. *J Mol Biol*, 2004. 338(4): p. 669-82.